Hydrothermal Conversion of Thorium Oxalate into ThO2 × nH2O Oxide

J. Manaud, Jérôme Maynadie, Adel Mesbah, Myrtille O J y Hunault, Philippe Martin, Morgan Zunino, Nicolas Dacheux, Nicolas Clavier

Hydrothermal conversion of thorium oxalate into $ThO_2 \cdot nH_2O$ oxide

Jérémie Manaud [1], Jérôme Maynadié [1], Adel Mesbah [1], Myrtille O.J.Y. Hunault [2], Philippe M. Martin [3], Morgan Zunino [1], Nicolas Dacheux [1], Nicolas Clavier [1,]*

[1] ICSM, Univ Montpellier, CEA, CNRS, ENSCM, Bagnols-sur-Cèze, France

[2] Synchrotron SOLEIL, L'Orme des Merisiers, Saint Aubin BP 48, 91192 Gif-sur-Yvette, France

[3] CEA, DES, ISEC, DMRC, Univ Montpellier, Marcoule, France

*** Corresponding author:**

Dr. Nicolas CLAVIER
ICSM, Univ Montpellier, CEA, CNRS, ENSCM
Site de Marcoule
BP 17171
30207 Bagnols sur Cèze
France

Phone : + 33 4 66 33 92 08
Fax : + 33 4 66 79 76 11

nicolas.clavier@icsm.fr

Abstract :

Hydrothermal conversion of thorium oxalate, $Th(C_2O_4)_2.nH_2O$, into thorium dioxide was explored through a multiparametric study, leading to some guidelines for the preparation of crystallized samples with the minimum amount of impurities. As the formation of the oxide appeared to be operated through the hydrolysis of Th^{4+} after decomposition of oxalate fractions, pH values typically above 1 must be considered to recover a solid phase. Also, due to the high stability of the thorium oxalate precursor, hydrothermal treatments of more than 5 hours at a temperature above 220°C were required.

All the $ThO_2.nH_2O$ samples prepared presented amounts of residual carbon and water in the range of 0.2-0.3 wt.% and $n \approx 0.5$, respectively. Combined FTIR, PXRD and EXAFS study showed that these impurities mainly consisted in carbonates trapped between elementary nanosized crystallites, rather than substituted directly in the lattice, which generated a tensile effect over the crystal lattice. The presence of carbonates at the surface of the elementary crystallites could also explain their tendency to self-assembly, leading to the formation of spherical aggregates. Hydrothermal conversion of oxalates could then find its place in different processes of the nuclear fuel cycle, where it will provide an interesting opportunity to set up dustless routes leading from ions in solution to dioxide powders in a limited number of steps.

1. Introduction

Actinide dioxides, such as UO_2 or $(U,Pu)O_2$ MOx, are used as fuels in a large majority of nuclear power plants worldwide. Their fabrication is mostly based on powder metallurgy that can lead to heterogeneities cationic distribution in the case of mixed oxides [1]. In order to overcome potential limitations due to this drawback [2], especially during the reprocessing steps during which insoluble PuO_2 aggregates can form [3,4], advanced fabrication schemes using wet chemistry processes have been investigated. They generally start from the precipitation of precursors in solution (e.g. hydroxides [5], carbonates [6], or carboxylates [7]), which are further converted into oxides by the means of a heat treatment.

In this context, actinide oxalates have drawn strong interest in the last decades [8] and oxalic precipitation is already used in France to recover plutonium in the spent fuel reprocessing process [9]. Indeed, the so-called oxalic conversion usually leads to the rapid and quantitative precipitation of cations in solution. Moreover, the very rich crystal chemistry of oxalate compounds allows the formation of mixed solid solution incorporating actinides under various oxidation states [10]. However, the oxide powders prepared through these methods can contain significant amounts of residual carbon (typically up to 0.1 wt.%, i.e. 2.2 at.%) coming from the decomposition of the organic fraction during the calcination step. It can even exceed the required levels for fuel fabrication (i.e. around 100 ppm) [11,12] and impact the sintering process. Also, powders frequently inherit the initial platelet morphology of the initial precursor, which could hamper the flowability of the powder during shaping process leading to green fuel pellets. As a consequence, less efficient densification and increased formation of macroscopic defects could be observed after sintering [12]. Considering these potential drawbacks, several research groups recently investigated the possibility of operating the "oxalate to oxide conversion" using mild hydrothermal conversion [13–16]. In this frame, actinide dioxides (with An(IV) = Th, U, Np and Pu) were prepared, generally as nanocrystalline powders, after heating oxalate counterparts in aqueous media under hydrothermal conditions for several hours in the 200-250°C range.

However, even if the successful preparation of AnO_2 samples provided the proof of concept for this method, the exact mechanism underlying the oxalate to oxide conversion in hydrothermal conditions still requires accurate description. Our previous work dedicated to uranium-based samples, showed that the conversion was first driven by the oxidative decomposition of oxalate entities, then by the hydrothermal reduction of U(VI) into U(IV),

that allowed the precipitation of the oxide through hydrolysis and ageing [16]. Redox processes then appeared of primary importance in the reaction scheme, but also impacted the chemistry of the oxide samples, the final O/U ratio being strongly dependent on the operating conditions, especially in terms of heating time, temperature and acidity of the medium.

In order to go further with hydrothermal conversion of An(IV) oxalates, a new study focused on thorium compounds was initiated. First, ThO_2 presents several physico-chemical properties of interest, such as higher thermal conductivity and melting point than UO_2, which can enhance the thermal yield and increase the tolerance to accidental situations. For all these reasons, ThO_2 could be envisaged as an alternative to UO_2 nuclear fuels. In this field, advanced projects of ThO_2-based fuel cycles are currently developed in several countries [17], including India [18] and China [19]. Second, with Th(IV) as the only stable oxidation state, it allows to avoid redox reactions and constitutes an interesting model for other actinide-based compounds. Indeed, several actinides such as U or Pu are also stabilized in the (+IV) oxidation state and crystallise as UO_2 or PuO_2 with the same fluorite structure as ThO_2. On this basis, a multi-parametric study dedicated to the conversion of thorium oxalate $Th(C_2O_4)_2.nH_2O$ into $ThO_2.nH_2O$ was undertaken, to unravel the impact of heating duration, temperature and pH on the physico-chemical characteristics of the final oxide. Particular attention was paid to the crystallographic structure of the samples, as well as to their morphology and the impurity content. After determining the optimal conditions leading to well-crystallized oxide, with the lowest level of impurities achievable, a detailed structural study using EXAFS was undertaken, particularly with the aim to provide new information regarding the location of residual carbon in the samples and to evaluate the impact of the nanostructuration.

2. Experimental

Caution! ^{232}Th is a α-emitter radioelement and considered as a health risk. Experiments involving thorium require appropriate facilities and trained persons in handling of radioactive materials.

2.1. Preparation of the samples

All the reagents used were of analytical grade and supplied by Sigma-Aldrich, except thorium nitrate pentahydrate, supplied by Ibilabs. The preparation of the thorium nitrate solution was performed by dissolving thorium salt in concentrated nitric acid (2M). The thorium concentration in the final solution was estimated to 0.170 ± 0.002 M using ICP-AES analyses.

The preparation of all the samples was based on the initial precipitation of thorium oxalate $Th(C_2O_4)_2.nH_2O$, and its conversion into $ThO_2.nH_2O$ under mild hydrothermal conditions. The oxalic precipitation of thorium was operated by mixing about 1 mmol of thorium in nitric solution with a 50 mol.% excess of 0.5 M oxalic acid. A white precipitate of $Th(C_2O_4)_2.6H_2O$ was immediately formed, then was magnetically stirred to reach an homogeneous dispersion in solution. Afterward, the suspension was transferred in a 23 mL Teflon-lined autoclave (Parr). The pH was generally found to be below 0.5, and was adjusted, when needed, by adding diluted NH_4OH (3.5 M) or 0.5 M hydrochloric acid. In any case, the volume of the solution was maintained to 15 mL in order to avoid any bias due to uncontrolled variations of autogenous pressure during the thermal treatment.

The reactor was heated between 130 and 250°C for 1 to 48 hours. The maximum pressure reached at 250°C was estimated to 80 bars [20]. After heating, the autoclave was cooled down to room temperature naturally. The final precipitate was first separated by centrifugation at 14000 rpm, then washed twice with deionized water and finally with ethanol prior final drying overnight at 90°C in an oven. At this temperature, previous studies already showed that the hydration rate of $MO_2.nH_2O$ (M = Th, U or Ce) samples was not modified, thus allowing us to avoid any bias during further characterization [5,21].

2.2. Characterization of the samples

PXRD. Powder X-Ray Diffraction (PXRD) diagrams were collected by the means of a Bruker D8 diffractometer equipped with a Lynx-eye detector adopting the reflexion geometry and using Cu $K\alpha_{1,2}$ radiation (λ = 1.54184 Å). PXRD patterns were recorded at room temperature in the 5 – 100° range (2θ), a step size of $\Delta(2\theta)$ = 0.01° and a total counting time of about 3 hours per sample. In order to avoid any radioactive contamination, the powders were placed in a special sample holder (dome-shaped container with anti-scattering blade) that could generate additional large peak between 10 and 20° (2θ). Pure silicon was collected as a standard and used to extract the instrumental function. All the PXRD patterns were

refined by the Rietveld method using the Cox-Hastings pseudo-Voigt profile function [22] implemented in the Fullprof_suite software [23]. During the refinements, the conventional profile/structure parameters (zero shift, unit cell parameters, scale factors, global thermal displacement and asymmetric parameters) could vary. Moreover, the modelling of the intrinsic microstructure parameters was performed by applying both an anisotropic size and strain model in agreement with the m-3m Laue class.

SEM observations. Before their observation, the samples were systematically deposited on a carbon adhesive tape. Scanning Electron Microscope (SEM) micrographs were then directly recorded from the as-deposited powders without any additional preparation such as metallization. A FEI Quanta 200 scanning electron microscope, equipped with an Everhart-Thornley Detector (ETD) and a Back-Scattered Electron Detector (BSED) was used to record images with an acceleration voltage of 30kV under high vacuum conditions (10^{-6} Pa).

TG-MS Analyses. Thermogravimetric analyses coupled with mass spectrometry were undertaken using a Setaram Setsys Evolution equipped with a type S thermocouple (Pt / Pt-10%Rh). After recording a baseline using an empty crucible (100 µL), weight loss was measured during a heat treatment up to 1000°C with a rate of 5°C.min^{-1} under air. Moreover, the gaseous species emitted during the heat treatment were analyzed by the means of Hiden Analytical QGA analyzer using mass spectrometry.

Carbon Analyses. The amount of residual carbon in the oxide powders was determined by the means of a LECO CS230 Carbon/Sulfur apparatus. In order to remove all adsorbed atmospheric CO_2, the samples were first dried overnight at 90°C in an oven. The complete combustion was then immediately performed under oxygen atmosphere and the concentration of CO_2 was further determined by IR absorption. In order to recover quantitative values, a blank and a series of standards (steels containing 0.0013 to 5.02 wt.% of carbon) were analyzed prior our samples.

FTIR spectroscopy. Fourier-Transform Infrared spectra were recorded in the 380-4000 cm^{-1} range using a Perkin-Elmer FTIR Spectrum 100 device. Powdered samples were deposited at the surface of an ATR crystal without any prior preparation. The spectra collected in such operating conditions exhibited a resolution lower than 2 cm^{-1}.

X-ray Absorption Spectroscopy (XAS). X-ray absorption spectra (XAS) were measured at the MARS beamline at the SOLEIL synchrotron (Saint-Aubin, France) [24,25]. The storage ring was operating in top-up mode at an electron current of 450 mA, 2.5 GeV. EXAFS was measured at the Th L_{III}-edge (16.3 keV) using a double-crystal monochromator (DCM) equipped with a pair of Si (220) crystals. Rejection of higher harmonics as well as vertical focusing was achieved using two platinum-coated mirrors under total reflection at 3.1 mrad, inserted before and after the DCM. The beam size on sample was 300 μm × 200 μm FWHM (H x V). The incident energy was calibrated using a metallic yttrium foil (K-edge at 17.038 keV). The EXAFS signal was measured in transmission mode using intensity monitors. At least 3 scans were recorded for each sample and scans were aligned in energy before a merge. After normalization, the fine structure oscillations were extracted from absorption signal using Athena software [26]. The occurrence of a double-electron excitation in the Th-L_{III}-edge EXAFS spectra was shown by Hennig and can affect the EXAFS signal and influence the data analysis, especially for the first coordination shell [27]. To avoid this phenomenon, the double-electron excitation contribution was removed by using the multi-electron excitation removal (MEE) of Athena software. The input parameters were first optimized using the ThO_2 reference spectrum and the following values were obtained: energy offset of 373 eV with 1 eV of broadening and 0.005 (relatively to the edge step) of amplitude. These parameters were then applied to correct the data collected for all our samples. The EXAFS spectra obtained before and after the correction are supplied as supplementary material (Figure S1). The Artemis software [26] was used for EXAFS fitting simultaneously in k^1, k^2 and k^3 using interatomic scattering path phases and amplitudes calculated by FEFF 8.40 ab initio code [26]. A fixed $S0_2$ value of 1.00, derived from ThO_2 fit, was used. Data were fitted by introducing the contribution of the four main scattering paths corresponding to the first three shells of atomic neighbors (Th-O_1, Th-Th, Th-O_2) and one multiple scattering (Th-O_1-Th-O_1-Th) in the simulation. The fit limits were taken from 3.5 to 13.7 $Å^{-1}$.

3. Results and Discussion

3.1. Effect of Temperature

The effect of the hydrothermal treatment temperature on the physico-chemical properties of the powders synthesized was first examined between 130 and 250°C. The duration of the hydrothermal treatment was arbitrarily set to 24 hours while the pH of the initial media was not modified and remained strongly acidic (*i.e.* pH < 0.5). Additionally, a thorium oxalate sample was also synthesized without any further hydrothermal treatment to act as a room temperature reference. It corresponds to the white precipitate initially formed after the mixture of the reactants.

The powders synthesized under hydrothermal conditions between 130°C and 250°C as well as the reference were first characterized by PXRD (**Figure 1**). Up to 170°C, all the samples prepared adopted the monoclinic structure (C2/c space group) reported by Clavier *et al.* for $Th(C_2O_4)_2.2H_2O$ [28]. Increasing the temperature in this domain only led to the narrowing of PXRD lines, as a consequence of the improvement of the crystallization. Owing to the drying conditions used in this work (i.e. T = 90°C, one night), it is important to underline that the formation of the dihydrated form of the oxalate is in good agreement with the literature that mentions the transition from $Th(C_2O_4)_2.6H_2O$ to $Th(C_2O_4)_2.2H_2O$ at low temperature [29,30].

From 180°C up to 250°C, no precipitate was observed after the 24-hour hydrothermal treatment. The starting dihydrated thorium oxalate then completely decomposed under these conditions, which probably also induced the decomposition of the oxalate moieties [31]. Nevertheless, the acidity of the reacting media did not allowed to form $Th(OH)_4$ then $ThO_2.nH_2O$ by aging, conversely to what we observed for uranium(IV) [16]. This observation was in good agreement with the hydrolysis constants which reach $\log_{10}K^0 = 46.7$ and 54.5 for Th^{4+} and U^{4+}, respectively [32,33]. Also, the fourth hydrolysis reaction, leading to the precipitation of $Th(OH)_4$ is usually reported to become prevailing only for pH ≥ 3 at room temperature [34]. The strongly acidic media resulting from the mixture of the reactants could thus avoid the formation of such thorium tetrahydroxide precipitate, indicating that the pH must be monitored to an upper value to succeed in the hydrothermal conversion of thorium oxalate into thorium dioxide.

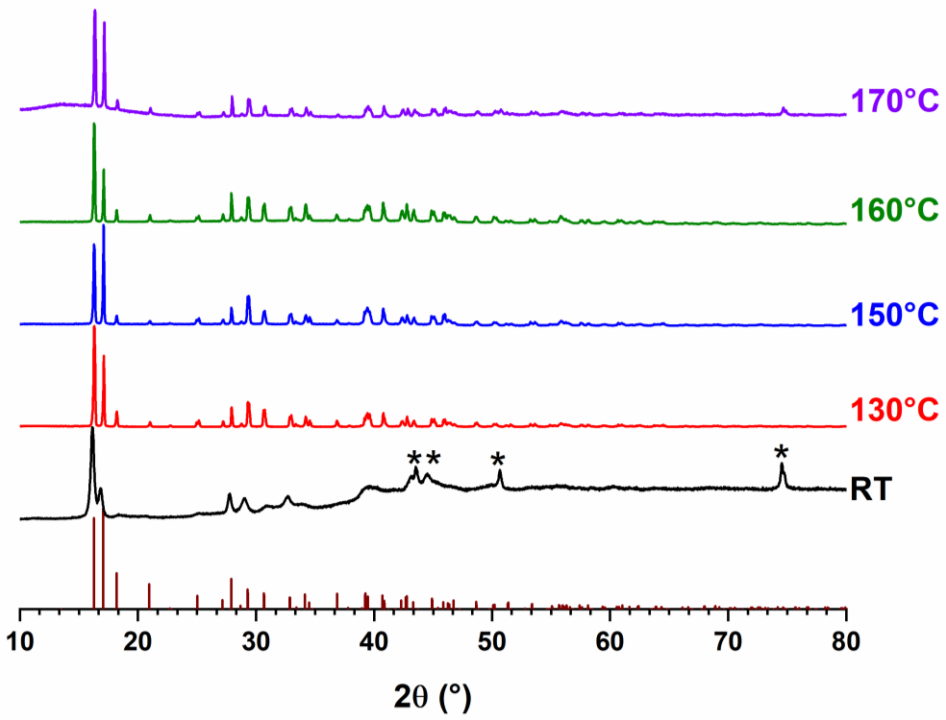

Figure 1. PXRD diagrams obtained after hydrothermal treatment of $Th(C_2O_4)_2.nH_2O$ at various temperatures (130-170°C) during 24h at pH < 0.5 and comparison with the sample prepared at room temperature. Stick pattern (brown) of $Th(C_2O_4)_2.2H_2O$ [35]. XRD lines associated to the sample holder are pointed out by asterisk.

3.2. Effect of initial pH

The effect of the pH was then studied in order to proceed to the thorium hydrolysis after the decomposition of the oxalate moieties. Based on the previous results obtained on uranium(IV) [16], the temperature of hydrothermal treatment was set to 250°C, which corresponds to the optimal conditions to prepare anhydrous dioxide samples showing low contents of carbon impurities. The duration of the hydrothermal treatment remained unchanged (i.e. 24 hours) while the pH of the initial mixture was adjusted between pH = 1 and pH = 8.

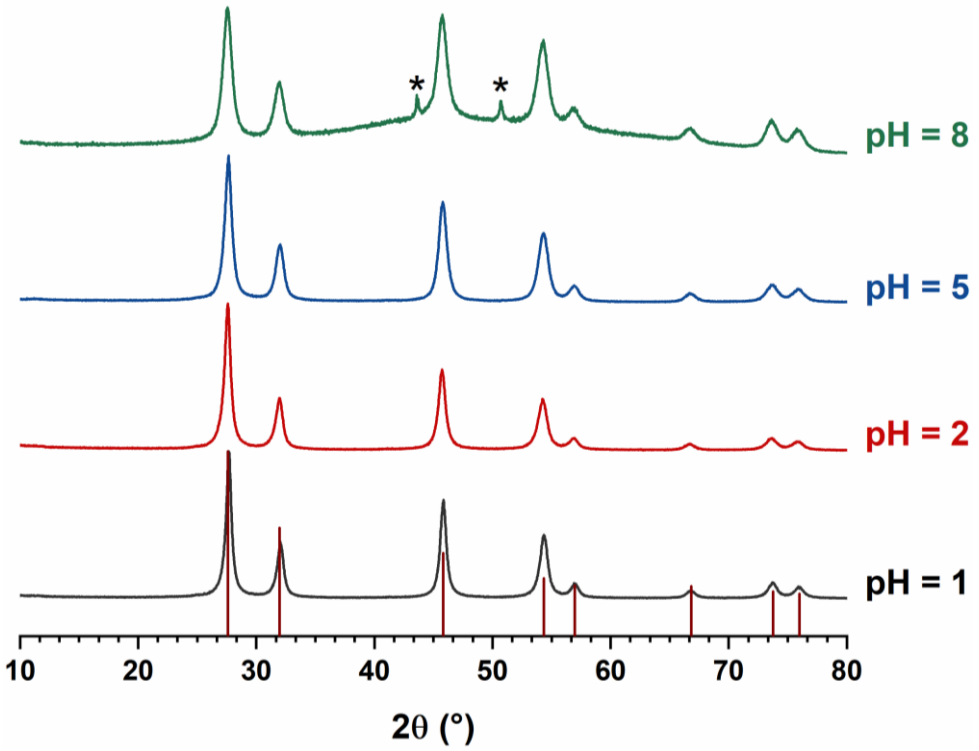

Figure 2. Variation of the PXRD patterns recorded for $ThO_2.nH_2O$ samples prepared by hydrothermal conversion of $Th(C_2O_4)_2.nH_2O$ (T= 250°C, t = 24 h) as a function of the starting pH value. Stick pattern (brown) of ThO_2 [28]. XRD lines associated to the sample holder are pointed out by asterisk..

The samples prepared were first characterized by PXRD (**Figure 2**). For all the conditions investigated, the characteristic PXRD lines of the fluorite-type structure (Fm-3m space group) of thorium dioxide were observed [36]. This indicated that $ThO_2.nH_2O$ compounds were obtained from the hydrothermal conversion of the oxalate precursor whatever the pH value considered. Indeed, it is important to remind that the pH of the reacting media was adjusted after the initial precipitation of thorium oxalate. This procedure ruled out any direct formation of thorium oxide for the higher pH values tested.

Additionally, the formation of thorium oxide was also achieved for starting pH values of 1 and 2, leading to a well crystallized sample, even if thorium hydrolysis was generally reported to be a significant process only for pH ≥ 3 at room temperature [34,37]. Increasing temperature and pressure through hydrothermal conditions here affected thermodynamics of hydrolysis and offered the possibility to quantitatively form thorium dioxide at lower pH values. The range of operating conditions allowing the hydrothermal conversion of thorium

oxalate was then probably larger than that reported by Walter *et al.* who only worked in distilled water [13].

In addition, Rietveld refinements of the PXRD data were performed in order to determine the unit cell volumes and average crystallite sizes and possible strain effect. The modification of the initial pH value between 1 and 5 first had a negligible impact on the variation of the unit cell volume (**Figure 3a**). Increasing pH to 8 also led to a very limited variation of only 0.15 ± 0.01 $Å^3$. However, for all the samples, the unit cell volume was about 1 $Å^3$ above the value usually reported for ThO_2 in the literature (175.43 ± 0.03 $Å^3$) [36]. This discrepancy could underline the presence of impurities in the powders such as water or carbon, already mentioned during the direct preparation of thorium dioxide through hydrothermal processes [38]. It could also be associated to a small size of crystallites, as nanostructured powders have been recently reported to present slightly higher unit cell volumes [39]. Indeed, the average crystallite size was typically found between 9 and 11 nm for our samples (**Figure 3b**). This range of values is almost four times lower than that reported by Clavier *et al.* for thorium dioxide samples directly prepared through hydrothermal conversion of thorium aspartate [38]. This difference could come from the differences in the complexing agent used (i.e. aspartate vs. oxalate) and the temperature applied for hydrothermal conversion (200°C vs. 250°C) : both parameters probably led to slow down the decomposition of the initial precipitate in the case of thorium aspartate, which further favored growth over nucleation during the formation of the oxide. Nevertheless, the average crystallite size determined in this study remains in the same order of magnitude than the 6nm-sized ThO_2 obtained by hydrothermal conversion of thorium oxalate [14] or than ThO_2 nanoparticles obtained by Bonato *et al.* when firing thorium oxalate between 485°C and 600°C [40]. On the other hand, conventional routes used for the preparation of ThO_2 powders, frequently based on the pyrolysis of thorium salts (e.g. nitrate, carbonate or hydroxide) at high temperature[41], are generally associated with microcrystalline powders, showing average crystallite size typically exceeding 100 nm.

a) **b)**

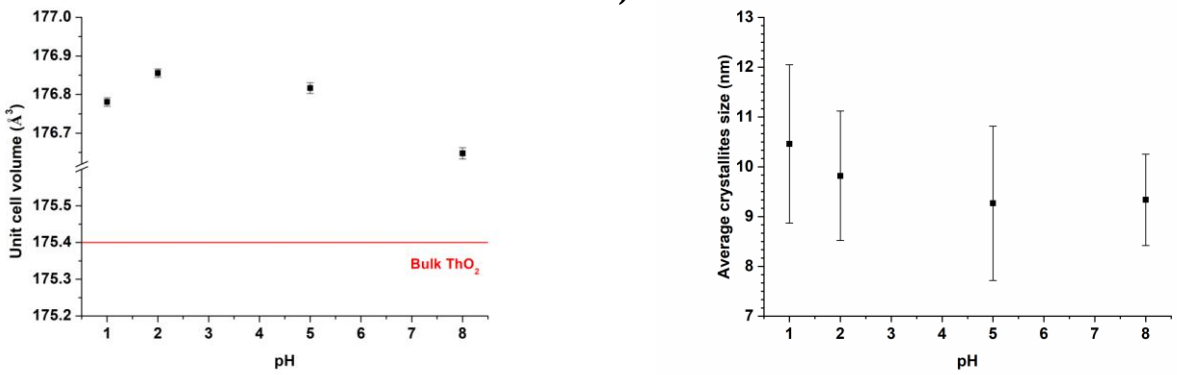

Figure 3. Variation of the unit cell volume (a) and of the average crystallite size (b) obtained for $ThO_2.nH_2O$ samples as a function of starting pH (T = 250°C, t = 24h). Standard error deviation for the unit cell volume is ± 0.01 $Å^3$.

The residual contents of carbon within ThO_2 samples were further evaluated for all the samples (**Table 1**). For pH values ranging from 1 to 5, residual carbon content reached an average value of 0.36 ± 0.06 wt. %. This content was close to that obtained by Clavier *et al.* (0.27 wt. %) when preparing ThO_2 from the hydrothermal conversion of thorium aspartate [38] but higher than those usually mentioned after thermal conversion (0.005 wt. %) [42]. For starting pH = 8, the residual carbon content was found to be even higher and reached 0.84 ± 0.01 wt. %. This observation could be associated with that of Crossey, who reported a strong slowdown of oxalate degradation when increasing the pH of the solution [31]. Whatever the amount of carbon measured, additional FTIR characterization (see **Figure S1** in supplementary information), showed that it remained in the samples as carbonates, most likely as an amorphous solid phase. Indeed, all the spectra exhibited two bands at around 1520 and 1350 cm^{-1}, associated with the antisymmetric vibration of C-O bonds [43]. The presence of carbonates as a result of the hydrothermal decomposition of oxalate groups is not surprising, owing to the carbonate or oxocarbonate reaction intermediates already reported during the thermal decomposition of actinide oxalates [9,29,44]. Also, carbonate species probably exists in solution, especially for the highest pH values considered, and could be co-precipitated during the formation of hydroxides nuclei. However, one must note that despite important variations in the carbon content between pH = 1 and pH = 8, the unit cell volume only appeared slightly affected: if the presence of impurities seems to impact the structural characteristics of the oxide samples, it is then mostly independent on their quantity in the 0.3-0.9 wt. % range.

Table 1. Carbon contents determined in the samples prepared by hydrothermal conversion of $Th(C_2O_4)_2.nH_2O$ (T = 250°C, t = 24 hours) for various starting pH.

Starting pH	1	2	5	8
C (wt.%)	0.40 ± 0.02	0.32 ± 0.02	0.36 ± 0.01	0.84 ± 0.01

Besides achieving the formation of thorium dioxide samples, the increase of the initial pH also led to the modification of the powders morphology. Indeed, as shown in **Figure 4**, the precipitated thorium oxalate initially exhibited the classical platelet-like habit widely described in the literature for An(IV) oxalates [45–48]. On the contrary, thorium dioxide samples systematically adopted a nearly spherical shape. At pH = 1 and 2, the morphology could be described as litchi-like aggregates, i.e. open hollow spheres, of less than 500 nm in diameter. At higher pH values, bigger aggregates of 1 to 2.5 µm in diameter, showing a spherical shape, were formed. Higher magnification (see **Figure S2** supplied as supplementary material) allowed us to evidence the aggregates surface texture, which confirmed they are composed by smaller crystallites, in good agreement with the results obtained from Rietveld refinement of PXRD data.

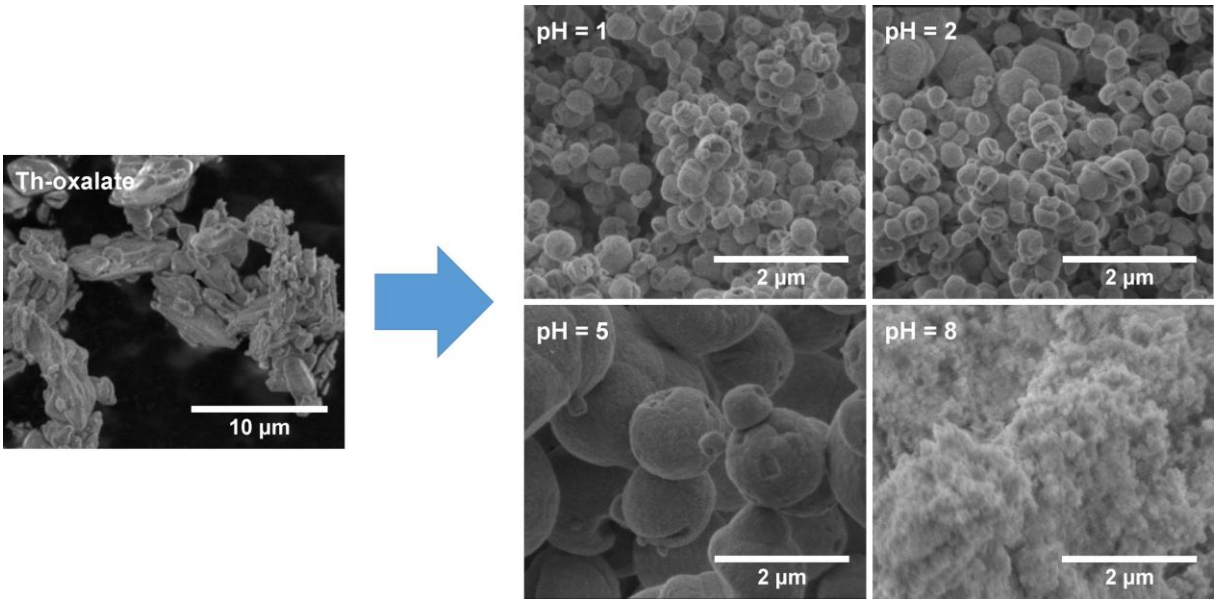

Figure 4. SEM micrographs of the $Th(C_2O_4)_2.2H_2O$ starting material prepared at room temperature (left) and of thorium dioxide samples synthesized under hydrothermal conditions from pH=1 to pH=8 (right).

Several authors, among who Tyrpekl *et al.*, already showed modifications in the morphology of thorium oxalate when varying the precipitation conditions (cation concentration, starting pH value, temperature…). They mentioned morphological changes from platelet-like particles to cubes or spheroids, which further impacted the morphology of the oxide formed after thermal conversion [45,46,49]. Also, few authors have already stated the one-step preparation of thorium dioxide samples with controlled morphology from the hydrothermal conversion of carboxylate precursors. Particularly, Balice *et al.* reported the formation of spherical aggregates of ThO_2 nanocrystallites of about 6-7 nm in size [14,15]. Such a spherical habit was probably driven by residual organic molecules adsorbed onto the powder surface. Similar processes were also reported recently by Clavier *et al.* when starting from thorium aspartate [38] or from uranium(IV) precursors, including oxalates and aspartates [16,50].

3.3. Effect of the duration of the hydrothermal treatment

The impact of the duration of the hydrothermal treatment on the physico-chemical properties of thorium dioxide samples prepared by hydrothermal conversion of $Th(C_2O_4)_2.nH_2O$ was studied in a next step. In order to prepare well crystallized $ThO_2.nH_2O$ with a spherical morphology, the temperature was kept to 250°C and the initial pH value was fixed to 5. The duration of the hydrothermal treatment was then varied from 1 to 48 hours.

All the powders obtained in such conditions were crystalline as illustrated by the PXRD patterns reported in **Figure 9**. However, if only the PXRD lines characteristic of ThO_2 were pointed out between 5 and 48 hours [36], the solid collected after 1 hour of hydrothermal treatment still consisted of a thorium oxalate. Nevertheless, the initial $Th(C_2O_4)_2.6H_2O$ evolved to the hexagonal $(NH_4)_2Th_2(C_2O_4)_5.1.5H_2O$ recently reported by Blanchard *et al*[51]. This transformation came from the use of NH_4OH to raise the pH value to 5 within the reacting media, and from further heating. Nevertheless, it is likely that the reactor did not reach thermal equilibrium in such a short time, hence that the average temperature of the reacting media was lower than 250°C. However, one must note that 1 hour of hydrothermal treatment in similar operating conditions was already proved to be sufficient to achieve the conversion of uranium (IV) oxalate into uranium oxide [16].

The one-pot conversion of thorium oxalates into thorium dioxide under hydrothermal conditions then appeared to be slower than that of the uranium(IV) compound. Considering the work reported by Crossey on the activation energy of oxalic acid decomposition (E_A = 207 kJ mol^{-1}) and assuming a similar first-order reaction, the decomposition of the oxalate should

be complete after 15 minutes at pH = 5 [31]. As such, the limiting parameter in the hydrothermal conversion of thorium oxalate is probably the stability of the oxalate phase itself. Such a stability, that is higher than that of its uranium(IV) counterpart [16], is probably inherited from the redox chemistry of the cation. Indeed, while thorium (IV) is stable, uranium (IV) can be easily oxidized to uranyl molecular ion.

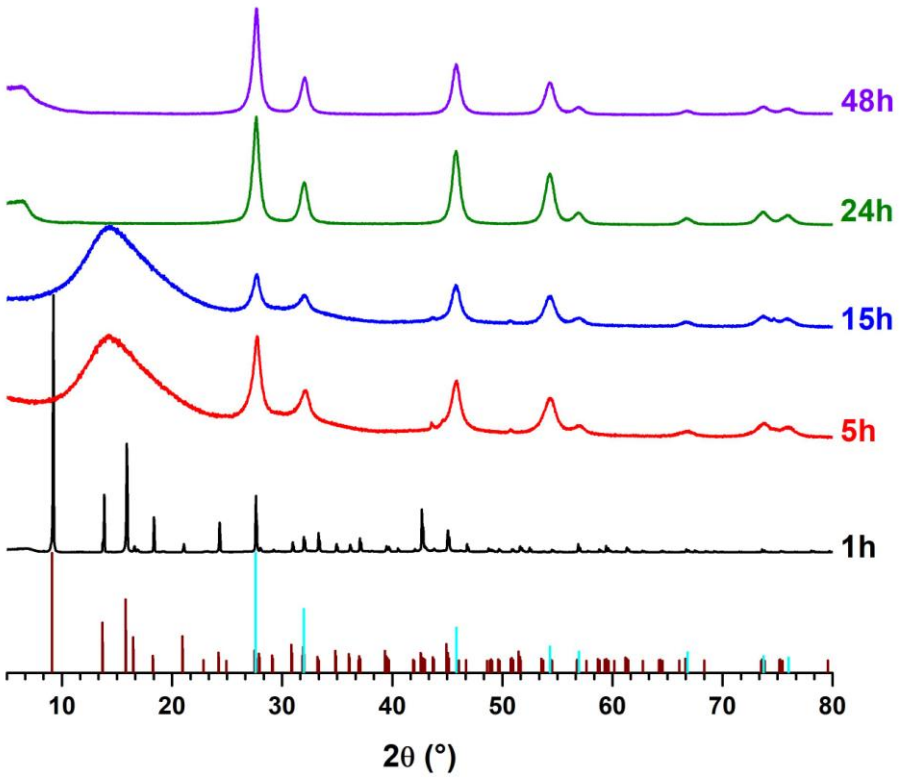

Figure 5. Evolution of the PXRD patterns obtained for samples prepared by hydrothermal conversion of $Th(C_2O_4)_2.nH_2O$ from 1 to 48 hours (T = 250°C, pH = 5): $(NH_4)_2Th_2(C_2O_4)_5.1.5H_2O$ was obtained for 1 hour and $ThO_2.nH_2O$ after 5 - 48 hours. Stick patterns of $(NH_4)_2Th_2(C_2O_4)_5.1.5H_2O$ (brown) [51] and ThO_2 (blue) [28].

Moreover, Rietveld refinements of the PXRD patterns revealed slight differences between the thorium dioxide samples formed after 5 to 48 hours of hydrothermal treatment (**Figure 6**). The largest unit cell volume was found to be 177.55 ± 0.01 $Å^3$ for 5 hours of heating then decreased down to a minimum of 176.80 ± 0.01 $Å^3$ after 24 hours. More generally, the samples prepared after 24 to 48 hours of hydrothermal treatment seemed to be the closest to the reference value of 175.43 ± 0.03 $Å^3$ [36], which could be linked to the elimination of impurities and/or defects. Such a process occurred jointly with the crystallite

growth, the average crystallite size being bigger for the powders prepared after 24 hours or 48 hours (10 – 14 nm) than those obtained after only 5 and 15 hours of hydrothermal treatment (6 – 8 nm). They still remained in good agreement with the results reported for a similar process of hydrothermal conversion (6 – 7 nm) [14,39]. Also, despite some differences in the average crystallite size, the morphology of the oxide samples still consists in spherical aggregates, in good agreement with the results reported in the previous section (see **Figure S3** supplied as supplementary material).

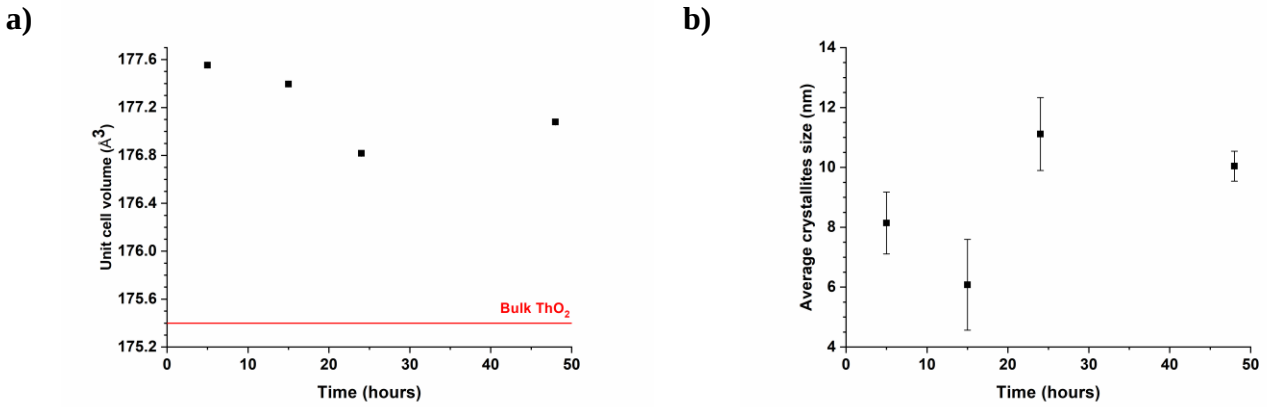

Figure 6 Evolution of the unit cell volume (a) and of the average crystallite size (b) obtained for $ThO_2.nH_2O$ samples prepared by hydrothermal conversion of $Th(C_2O_4)_2.nH_2O$ from 1 to 48 hours (T = 250°C, pH = 5). Standard error deviation for the unit cell volume is ±0.01 $Å^3$.

The presence of impurities within the powders was then checked in order to quantify the amounts of residual carbon and water coming from the hydrothermal degradation of $Th(C_2O_4)_2.nH_2O$. In agreement with the PXRD data which showed the formation of ammonium-thorium oxalate, the sample obtained after 1 hour of hydrothermal treatment presented a very high carbon content (**Table 2**). After 5 hours, it dropped down to 0.65 ± 0.01 wt. %, which fitted with the formation of thorium dioxide. Nevertheless, complementary FTIR analyses revealed that the characteristic vibration bands of oxalate groups could still be detected in this sample (**Figure 7**). Indeed, the $\nu_{as}(CO)$ mode around 1600 cm^{-1}, as well as the $\nu_s(CO)$ doublet at 1310 and 1350 cm^{-1}, which are the most intense vibration bands observed for the $(NH_4)_2Th_2(C_2O_4)_5.1.5H_2O$ sample formed after 1 hour of hydrothermal treatment, are still visible, although less intense. These signals further vanished when increasing the duration of the hydrothermal treatment, correlatively with the amount of residual carbon. This latter reached 0.28 ± 0.02 wt. % after 48 hours. At this stage, only carbonate species coming from the oxalate decomposition remained trapped in the samples. Also, these amounts were in good

agreement with those reported for ThO_2 samples prepared by hydrothermal conversion of carboxylate precursors [38] but remained more than 10 times higher than those reported for oxides issued from thermal conversion of oxalate under oxidizing atmosphere [42,47]. They also appeared to be significantly higher than the carbon contents reported in our previous work regarding the uranium(IV) system (i.e. typically less than 0.1 wt.%, *i.e.* 2.2 at.%) [16]. This difference might arise from the role played by the organic matter in the hydrothermal conversion of uranium oxalate, where carbon species are thought to reduce U(VI) into U(IV) prior to hydrolysis of the cation. As a consequence, their oxidation probably favor their elimination from the solid phase.

Table 2. Carbon and water contents determined in the samples obtained by hydrothermal conversion of $Th(C_2O_4)_2.nH_2O$ (T = 250°C, pH = 5) for various holding times.

Holding time (hours)	Total weight loss at 1000°C (%)	C (wt.%)	H_2O (wt.%)	H_2O (mol. per unit formula)
1	48.78 ± 0.05	11.10 ± 0.02	8.26 ± 0.05	4.7 ± 0.01
5	4.83 ± 0.05	0.65 ± 0.01	4.18 ± 0.05	0.64 ± 0.01
15	4.00 ± 0.05	0.38 ± 0.02	3.62 ± 0.05	0.55 ± 0.01
24	2.66 ± 0.05	0.36 ± 0.02	2.30 ± 0.05	0.35 ± 0.01
48	3.17 ± 0.05	0.28 ± 0.02	2.89 ± 0.05	0.44 ± 0.01

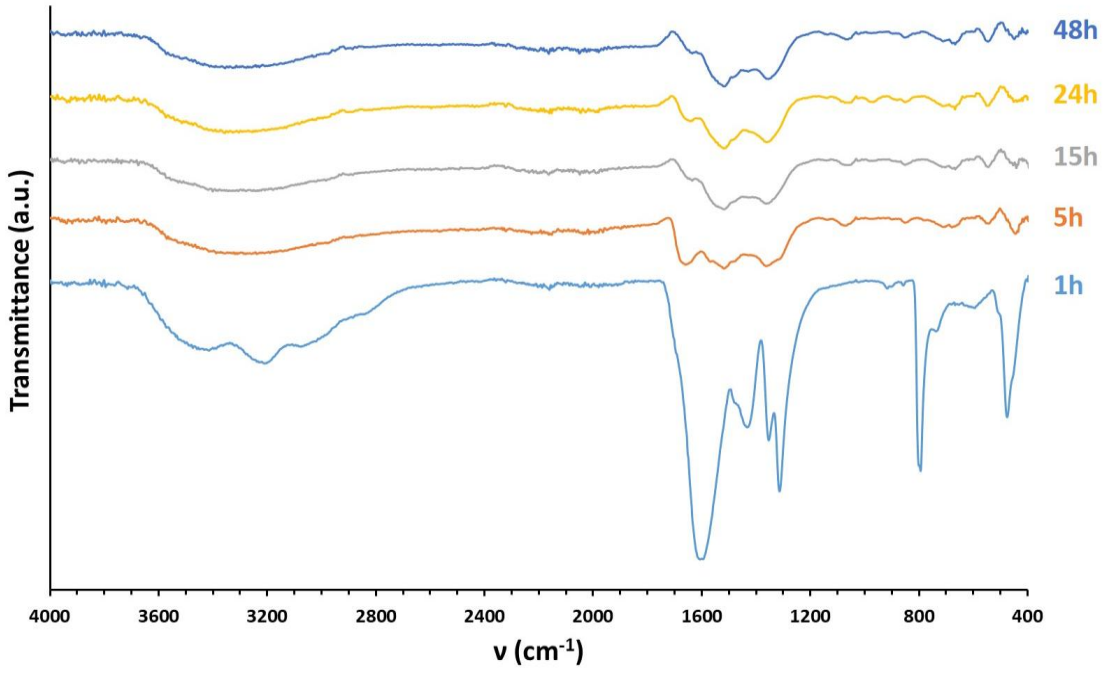

Figure 7. FTIR spectra of samples obtained from the hydrothermal conversion of $Th(C_2O_4)_2.nH_2O$ at T = 250°C and pH = 5, during 1 to 24 hours.

Furthermore, thermogravimetric experiments were undertaken in air in order to determine the water content in the oxide samples and to monitor the elimination of residual carbon (**Figure 8**). As expected, the thorium oxalate collected after 1 hour of hydrothermal treatment exhibited the highest relative weight loss. Based on MS analyses and the literature on the uranium counterpart $(NH_4)_2U_2(C_2O_4)_5.0.7H_2O$ [46], the first weight loss starting at 25°C and up to 200°C was assigned to the dehydration of the sample and the departure of ammonia. It was followed by a second weight loss associated to the decomposition of the oxalate moieties into a mixture of CO and CO_2 between 250°C and 600°C. The final weight loss reached about 50%, which appears in good agreement with the complete decomposition of $(NH_4)_2Th_2(C_2O_4)_5.nH_2O$, although the hydration rate determined herein (n ≈5), was found to be higher than that reported in the literature[44,51].

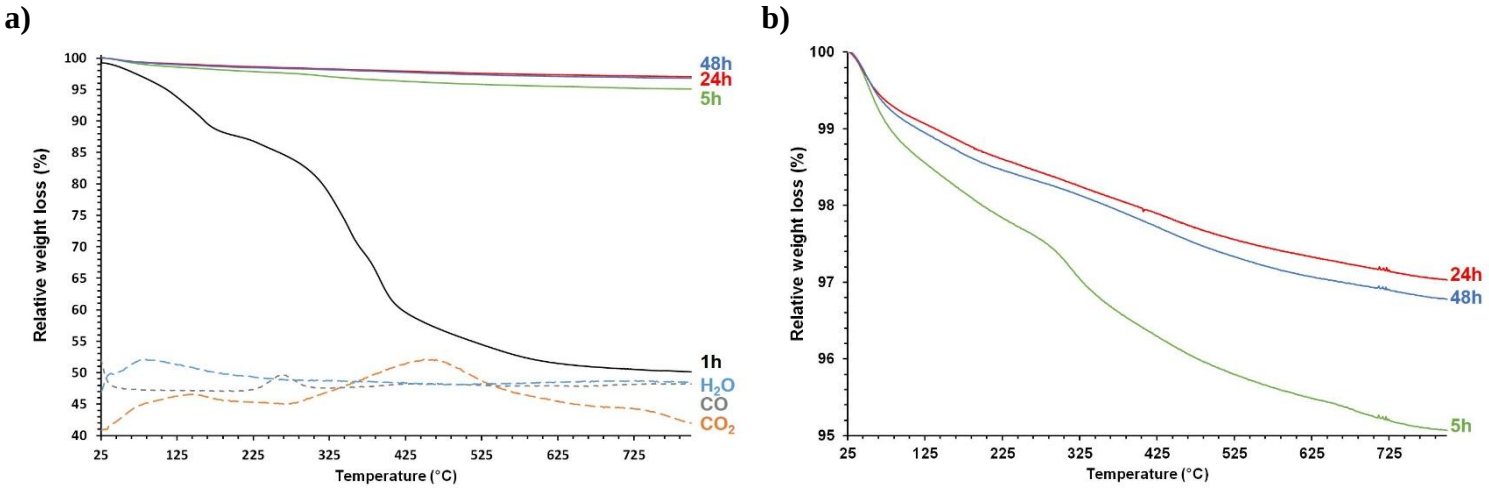

Figure 8. TG analyses of the samples formed through hydrothermal treatment of $Th_2(C_2O_4).nH_2O$ (250°C, pH = 5) during 1h, 5h, 24h and 48h. Associated mass spectroscopy analysis of emitted gases is presented for the sample prepared after 1h (H_2O : m/z = 18 - light blue dotted line; CO_2 : m/z = 44 - orange dotted line; CO : m/z = 28 – purple dotted line) (a). Focus of the curves obtained for 5h, 24h and 48h (b).

For longer durations of hydrothermal treatment, the total weight loss observed was much smaller and reached between 2.5 wt.% and 5 wt.%. However, the sample prepared after 5 hours presented the two-step behavior previously described for thorium oxalate, which could indicate that even if they were not detected by PXRD, some oxalates could remain in

this sample. Also, considering the amount of residual carbon in the sample and the weight loss measured, the hydration rate was estimated to 0.64 ± 0.01 H_2O per mole of ThO_2 for this sample. This value further decreased down to about 0.40 ± 0.05 H_2O per mole of ThO_2 when extending the duration of the hydrothermal treatment to 24 to 48 hours. It is worth noting that these values were in good agreement with the hydration rates generally reported in the literature for thorium dioxide samples formed by ageing of hydroxides, which is the most probable process driving the formation of ThO_2 consequently to the decomposition of thorium oxalate [52].

3.4. Impact of temperature when operating at pH = 5

Previous experiments led us to fix the starting pH and the duration of the hydrothermal treatment to pH = 5 and t = 24h, respectively, which allowed to prepare crystallized $ThO_2.nH_2O$ powders with the lowest amounts of impurities (i.e. carbon and water). The last set of experiments was then dedicated to the optimization of the synthesis temperature required for the one-pot conversion of $Th(C_2O_4)_2.nH_2O$ into $ThO_2.nH_2O$. As previously discussed, a particular attention was focused on the amount of residual carbon or water in the samples and on the variation of the unit cell volume which was always found up to now higher than the reference value of ThO_2. With this objective, the hydrothermal conversion of $Th(C_2O_4)_2.nH_2O$ was achieved for temperatures varying between 180°C and 250°C.

All the powders prepared in such conditions were found to be crystalline but presented different structures (**Figure 9**). At 180°C, the powder exhibited the PXRD lines of $(NH_4)_2Th_2(C_2O_4)_5.1.5H_2O$ whereas at 200°C, additional peaks evidencing the formation of $ThO_2.nH_2O$ were found at 28°, 32°, 46° and 54° (2θ). Above 200°C, only the PXRD lines of thorium dioxide were observed in such operating conditions (pH = 5 ; t = 24h). $ThO_2.nH_2O$ was then directly synthesized by hydrothermal conversion of $Th(C_2O_4)_2.nH_2O$ from 220°C to 250°C. One must note that this range of temperatures appeared to be slightly below that reported by Popa *et al.* who only obtained ThO_2 at 250°C [14].

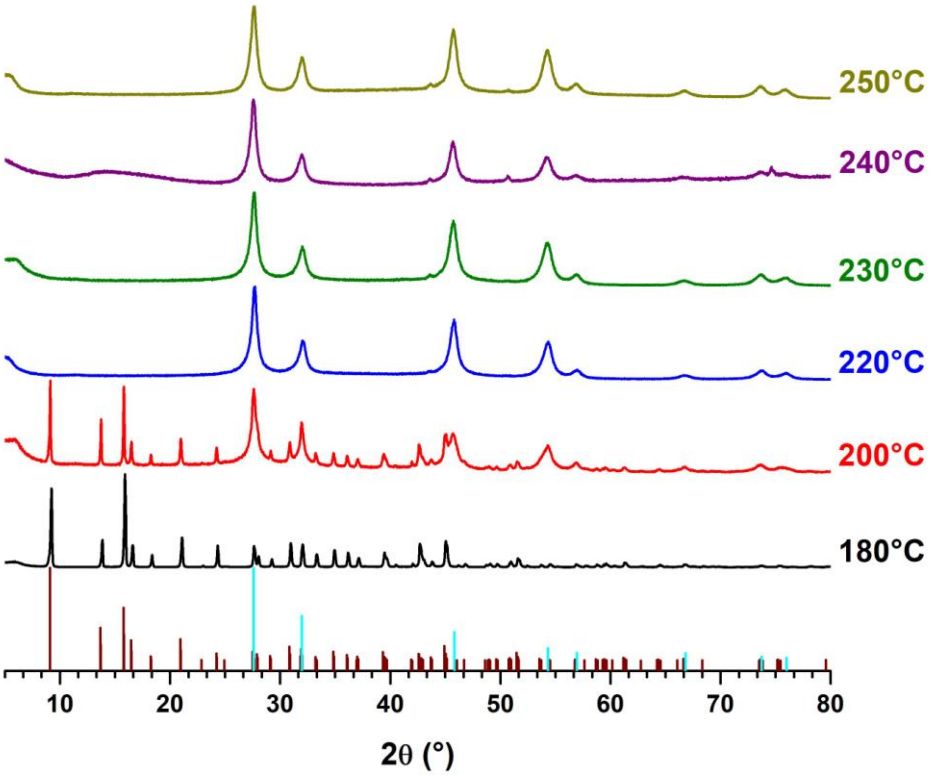

Figure 9. PXRD diagrams obtained after hydrothermal treatment of $Th(C_2O_4)_2.nH_2O$ at various temperatures during 24 h and for pH = 5. Stick patterns of $(NH_4)_2Th_2(C_2O_4)_5.1.5H_2O$ (brown) [51] and ThO_2 (blue) [28].

Then, the unit cell volume and the average crystallite size were determined by Rietveld refinements (**Figure 10**). The unit cell volume was found to decrease with the synthesis temperature down to 176.8 ± 0.01 $Å^3$ at 250°C, which still remained higher than the reference value reported for bulk ThO_2 [36]. Once again, the presence of impurities such as residual carbon or water molecule could explain this value [39] as well as the nanosized character of our samples, the average crystallite size remaining close to 10 nm. Indeed, based on this value, the unit cell volume determined in this work appeared to be in very good agreement with the data recently reported by Plakhova *et al.* [39].

a) **b)**

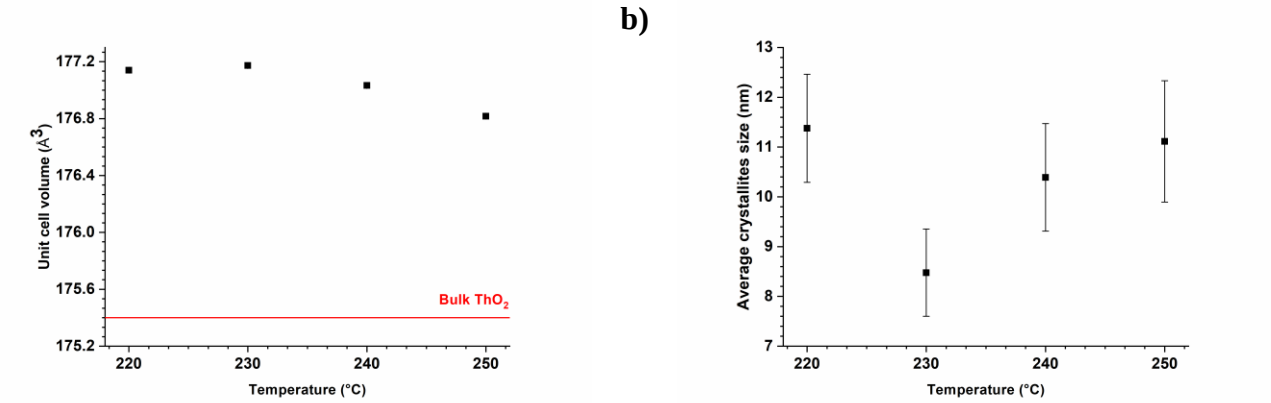

Figure 10. Variation of the unit cell volume (a) and of the average crystallite size (b) obtained from $Th(C_2O_4)_2.nH_2O$ as a function of temperature of the hydrothermal treatment (pH = 5, t = 24h). Standard error deviation for the unit cell volume is ±0.01 $Å^3$.

In parallel, carbon and water contents in the oxide samples were determined (**Table** 3). The carbon content reached 0.8-1 wt. % for thorium dioxides prepared at 220°C and 230°C. As it was evidenced previously for samples prepared for short hydrothermal treatment durations, such high carbon amounts were associated to the presence of remaining oxalate groups in the samples. These latter were evidenced on FTIR spectra by the large $\nu_{as}(CO)$ band around 1600 cm^{-1}, and the $\nu_s(CO)$ doublet at 1310 and 1350 cm^{-1} (**Figure 11**). The carbon content was further divided by 2 when raising the temperature up to 240°C and 250°C (0.40 ± 0.02 wt. % and 0.36 ± 0.02 wt. %, respectively). Simultaneously, the water content reached a minimum value of 0.35 ± 0.01 mole of H_2O per ThO_2 unit at 250°C. Thus, the amounts of carbon or water were found to be much higher (i.e. up to four times) in the prepared thorium dioxide than in uranium oxide synthesized by the same hydrothermal process [16]. Carbon coming from the oxalate decomposition was then not fully eliminated by the hydrothermal process whatever the temperature considered.

Table 3. Carbon and water contents determined in the samples prepared by hydrothermal conversion of $Th(C_2O_4)_2.nH_2O$ (t = 24h, pH = 5) for various temperatures of synthesis.

Temperature (°C)	Total weight loss at 1000°C (%)	C (wt.%)	H_2O (wt.%)	H_2O (mol. per unit formula)
220	N.D.	0.80 ± 0.01	N.D.	N.D.
230	N.D.	0.95 ± 0.01	N.D.	N.D.
240	3.38 ± 0.05	0.40 ± 0.02	2.98 ± 0.05	0.45 ± 0.01
250	2.66 ± 0.05	0.36 ± 0.02	2.30 ± 0.05	0.35 ± 0.01

N.D. : not determined

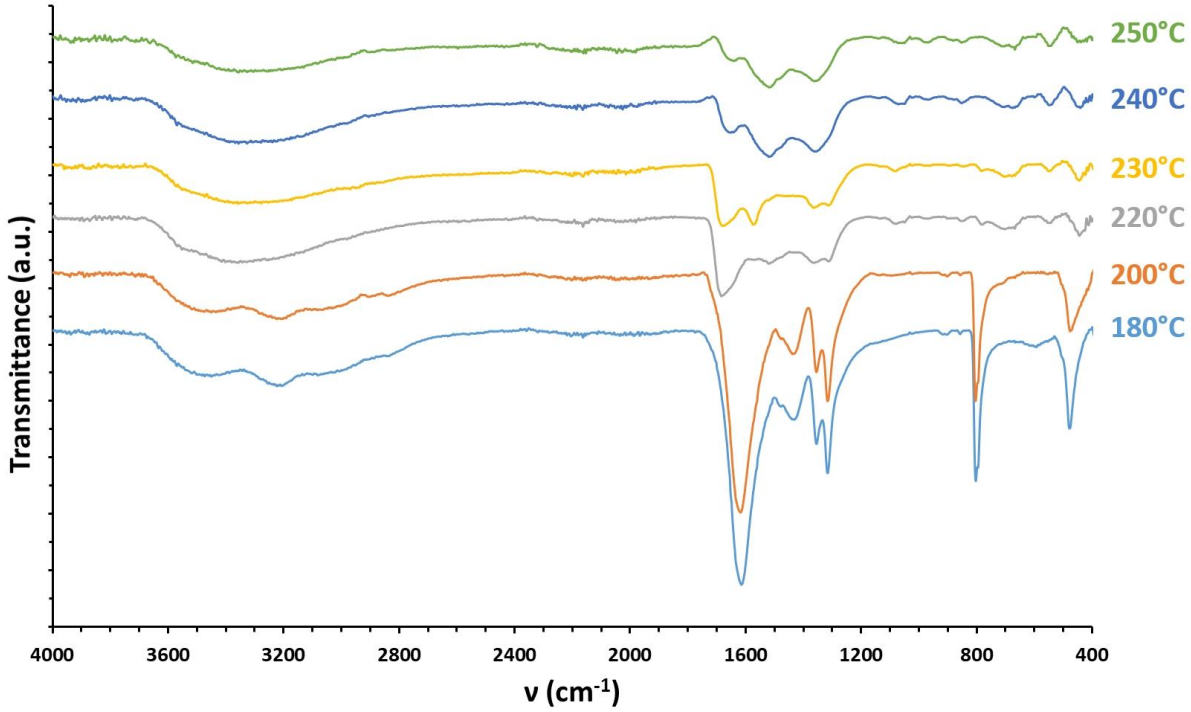

Figure 11. FTIR spectra of samples obtained from the hydrothermal conversion of $Th(C_2O_4)_2.nH_2O$ between 180 and 250°C (pH = 5, t = 24 hours).

In order to evaluate the impact of these impurities on the structure of ThO_2, and to get further insight on the location of carbon in the sample, a complementary EXAFS study was performed to characterize the local environment of the thorium cation for samples prepared at various temperatures (220°C, 240°C and 250°C).

A ThO_2 reference was taken from the thermal conversion of $Th(C_2O_4)_2.6H_2O$ at 1000°C for 2 hours under air. The Fourier Transform of the EXAFS data collected from the

oxide samples prepared by hydrothermal conversion of oxalate precursor are compared with ThO_2 in **Figure 12**. The first peak at about 2 Å corresponds to the apparent distance of the first shell Th-O_1 while the second peak at about 4 Å is mainly due to the first Th-Th with a small contribution of the second Th-O_2 shells. The main difference between the reference and our samples appears to be the FT magnitude, which is linked to the coordination number and/or disorder (Debye-Waller factor). The first peak of the Th-O_1 shell is close to that of the ThO_2 reference whereas the second peak of the Th-Th and Th-O_2 shells appears to be more impacted by the hydrothermal treatment with a higher difference between samples and reference data. The fit results are given in **Table 4**.

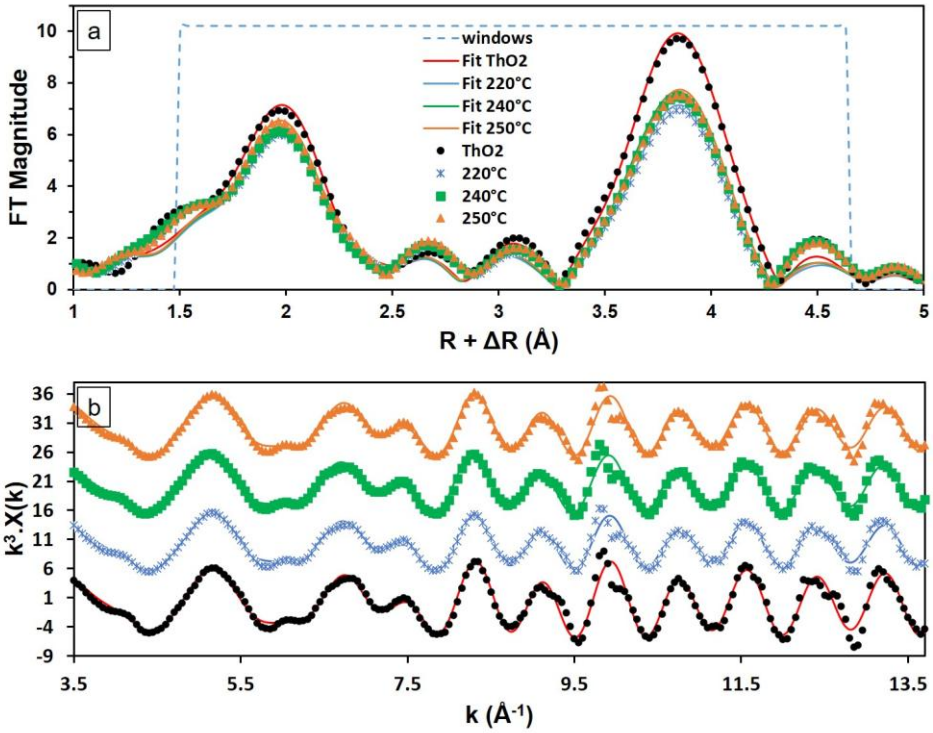

Figure 12. Thorium L_{III} edge k^3-weighted EXAFS data (b) and Fourier Transform (a) for each sample at the thorium L_{III} edge including best fits. The window indicates the fit limits. The FT window was taken over the *k*-space range 3.5 and 13.7Å^{-1} and magnified by k^3.

Table 4. Best fit results for the first three coordination shells at the thorium L_{III} edge.

			First shell			Second shell			Third shell		
			Th-O_1			Th-Th			Th-O_2		
	R-factor	ΔE_0 (eV)	N	R (Å)	$\sigma^2 \times 10^3$ (Å^2)	N	R (Å)	$\sigma^2 \times 10^3$ (Å^2)	N	R (Å)	$\sigma^2 \times 10^3$ (Å^2)
XRD data	-	-	8	2.4263	-	12	3.9621	-	24	4.6459	-
ThO_2 reference	0.005	5.3(9)	8	2.429(4)	9(1)	12	3.959(3)	4.8(6)	24	4.65(2)	11(4)
220°C	0.008	5(1)	7.6(3)	2.429(4)	10(4)	9.6(6)	3.958(4)	5.4(9)	15(4)	4.67(3)	12(9)
240°C	0.008	3(1)	7.7(3)	2.430(5)	9(1)	9.9(6)	3.959(4)	5.2(9)	18(4)	4.67(3)	13(9)
250°C	0.007	5(1)	7.9(3)	2.429(5)	9(1)	10.8(6)	3.958(4)	5.5(8)	20(4)	4.66(2)	13(7)

No variation was observed for the Debye-Waller factor σ^2 linked to the thermal agitation of the structure and its value was found to be close to that of bulk ThO_2 [53,54], confirming the very good crystallinity of the samples and the lack of significant amounts of structural defects. For the first shell Th-O_1, the hydrothermal treatment or the temperature used had no significant impact. Indeed, the coordination number N was systematically close to 8, while the interatomic distance was found to be in very good agreement with that of the ThO_2 reference. For the Th-Th shell, the interatomic distance measured remained also consistent with that of the reference. However, the coordination number was impacted by the temperature of the hydrothermal treatment. Indeed, the N value was found to about 10-11 instead of 12. This lower value was well explained by the nanometric size of our samples for which the surface was predominant over the core, leading the average number of neighbors lower than that observed in a bulk ThO_2 sample. As a matter of fact, a simple calculation based on the average crystallite sizes (*i.e.* around 10 nm) showed that 50 to 60% of the thorium atoms in the samples were located at the surface. A similar observation was made for the Th-O_2 shell: all the N values determined were significantly lower than that of ThO_2 reference (24), which confirmed once again the nanostructuration of the powdered samples. Moreover, the N value was found to increase with the temperature of the hydrothermal treatment, indicating that the size of nanoparticles increased. It was also in good agreement with the variation of the crystallite size determined by Rietveld refinement of PXRD data and with the decrease of the unit cell volume. This crystal growth still did not have any impact on the crystallographic structure since the interatomic distances and Debye-Waller factors remained close to their reference value in ThO_2.

The first shell Th-O_1 clearly fit with that of a crystalline ThO_2 without any modification of the EXAFS signal. Owing to the contents measured in our samples (typically in the 0.5-1 wt.% range i.e. 3-7 at.%), residual carbon species then cannot be mainly located within the crystal structure of ThO_2, even if the insertion of very limited amounts of C in the fluorite-type lattice cannot be ruled out. Correlatively, the residual carbon and water molecules are more likely adsorbed onto the surface of the nanosized crystallites, where they could generate a tensile effect over the crystal lattice, as recently proposed by Plakhova *et al.* [39]. Therefore, the organic matter residue was probably present as an amorphous form without any specific orientation, but with a huge disorder that did not affect the first neighbor coordination shell of O.

4. Conclusion

The multi-parametric study of the hydrothermal conversion of thorium oxalate $Th(C_2O_4)_2.nH_2O$ into thorium dioxide allowed us to draw some guidelines for the preparation of crystalline samples with minimum carbon and water contents. First, as the formation of ThO_2 appeared to be operated through the hydrolysis of Th^{4+}, pH values typically above 1 must be considered in order to recover a solid phase. Also, the minimum hydrothermal treatment duration was 5 hours, which showed the higher stability of the thorium oxalate precursor compared to its uranium(IV) counterpart. This feature was also evidenced by the temperature required to achieve the conversion, which reached 220°C (compared to only 180°C for uranium oxalate).

As a side effect, the important stability of thorium oxalate precursor led to higher amounts of residual carbon, present as carbonates and water in the oxide-based phases, i.e. typically in the range of 0.2-0.3 wt.% and around 0.5 mole per ThO_2, respectively. Although these contents were significantly higher than those reported during the conversion of $U(C_2O_4)_2.nH_2O$, they did not modify the structural features of the final oxides. Indeed, in-depth analysis using EXAFS spectroscopy systematically showed that the average Th-O and Th-Th distances were not modified for all the conditions of conversion tested, i.e. independently of the carbon amount. In the same time, the decrease of the coordination number in the second shell for low temperatures of conversion highlighted the nanocrystalline character of the powdered samples. Residual carbon then appeared to be trapped between nanosized crystallites rather than substituted directly in the lattice. As a result, it probably

generated a tensile effect over the lattice, which can explain the unit cell volume determined by PXRD, slightly above the values usually reported in the literature for bulk ThO_2. The presence of carbon at the surface of the elementary crystallites could also explain their tendency to form spherical aggregates, as adsorbed organic matter generally promotes self-assembly. Comparison with platelets ThO_2 nanoparticles prepared from a thermal calcination of oxalate shows that hydrothermal process allowed to stabilize in one-step better crystalline spherical ThO_2 nanoparticles at lower temperature.

The general behavior of actinide oxalates during hydrothermal conversion into actinide dioxide then appeared to be driven both by the stability of the precursor and by the tendency of the cation towards hydrolysis. In this sense, it should be significantly enhanced for tetravalent actinides presenting a smaller ionic radius than 1.05Å for Th^{4+}, e.g. Np^{4+} (0.98Å) and Pu^{4+} (0.96Å) [55]. Hydrothermal conversion of oxalates then could find its place in different processes of the nuclear fuel cycle, where it could provide an interesting opportunity to set up dustless routes leading from ions in solution to dioxide-based powders in a limited number of steps. Additional experiments are now under progress to extend this hydrothermal process to other systems of interest, including uranium-based mixed oxides.

Acknowledgements

Authors are grateful to J. Lautru for his help during SEM observations and B. Corso for his advice about PXRD analyses. They thank the SOLEIL synchrotron for providing beamtime. They would also like to thank the Materials Federative Project included in the NEEDS program (Nucléaire, Energie, Environnement, Déchets, Société) of CNRS for its continuous financial support.

Supporting information

FTIR spectra of thorium oxide samples synthesized from the hydrothermal conversion of oxalate precursor at various pH. SEM micrographs of oxide samples prepared at various pH (T = 250°C, t = 24 hours) and different hydrothermal treatment durations (T = 250°C, pH = 5). Thorium L_{III} edge k^3-weighted EXAFS data for ThO_2 and Fourier Transform of the EXAFS signal before and after the correction of the double-electron excitation contribution on the EXAFS spectra.

References

(1) Oudinet, G.; Munoz-Viallard, I.; Aufore, L.; Gotta, M.-J.; Becker, J. M.; Chiarelli, G.; Castelli, R. Characterization of Plutonium Distribution in MIMAS MOX by Image Analysis. *J. Nucl. Mater.* **2008**, *375* (1), 86–94. https://doi.org/10.1016/j.jnucmat.2007.10.013.

(2) Claparede, L.; Clavier, N.; Mesbah, A.; Tocino, F.; Szenknect, S.; Ravaux, J.; Dacheux, N. Impact of the Cationic Homogeneity on $Th_{0.5}U_{0.5}O_2$ Densification and Chemical Durability. *J. Nucl. Mater.* **2019**, *514*, 368–379. https://doi.org/10.1016/j.jnucmat.2018.12.009.

(3) Machuron-Mandard, X.; Madic, C. Basic Studies on the Kinetics and Mechanism of the Rapid Dissolution Reaction of Plutonium Dioxide under Reducing Conditions in Acidic Media. *J. Alloys Compd.* **1994**, *213–214*, 100–105. https://doi.org/10.1016/0925-8388(94)90887-7.

(4) Nikitina, G. P.; Zhukova, I. N.; Egorova, V. P. Dissolution of plutonium dioxide in nitric acid. *Radiokhimiya* **1995**, *37* (3), 210–213.

(5) Martinez, J.; Clavier, N.; Mesbah, A.; Audubert, F.; Le Goff, X. F.; Vigier, N.; Dacheux, N. An Original Precipitation Route toward the Preparation and the Sintering of Highly Reactive Uranium Cerium Dioxide Powders. *J. Nucl. Mater.* **2015**, *462*, 173–181. https://doi.org/10.1016/j.jnucmat.2015.03.053.

(6) Tae-Joon, K.; Kyung-Chai, J.; Jin-Ho, P.; In-Soon, C.; Cheong-Song, C. Crystallization Characteristics of Ammonium Uranyl Carbonate (AUC) in Ammonium Carbonate Solutions. *J. Nucl. Mater.* **1994**, *209* (3), 306–314. https://doi.org/10.1016/0022-3115(94)90268-2.

(7) Loiseau, T.; Mihalcea, I.; Henry, N.; Volkringer, C. The Crystal Chemistry of Uranium Carboxylates. *Coord. Chem. Rev.* **2014**, *266–267*, 69–109. https://doi.org/10.1016/j.ccr.2013.08.038.

(8) Abraham, F.; Arab-Chapelet, B.; Rivenet, M.; Tamain, C.; Grandjean, S. Actinide Oxalates, Solid State Structures and Applications. *Coord. Chem. Rev.* **2014**, *266–267*, 28–68. https://doi.org/10.1016/j.ccr.2013.08.036.

(9) Vigier, N.; Grandjean, S.; Arab-Chapelet, B.; Abraham, F. Reaction Mechanisms of the Thermal Conversion of Pu(IV) Oxalate into Plutonium Oxide. *J. Alloys Compd.* **2007**, *444–445*, 594–597. https://doi.org/10.1016/j.jallcom.2007.01.057.

(10) Vaudez, S.; Belin, R. C.; Aufore, L.; Sornay, P.; Grandjean, S. A New Fabrication Route for SFR Fuel Using (U, Pu)O_2 Powder Obtained by Oxalic Co-Conversion. *J. Nucl. Mater.* **2013**, *442* (1), 227–234. https://doi.org/10.1016/j.jnucmat.2013.08.023.

(11) Asakura, K.; Takeuchi, K. Effect of Residual Carbon on the Sintering Behavior of MOX Pellets. *J. Nucl. Mater.* **2006**, *348* (1), 165–173. https://doi.org/10.1016/j.jnucmat.2005.09.016.

(12) Chambon, C.; Vaudez, S.; Heintz, J.-M. De-Densification Mechanisms of Yttria-Doped Cerium Oxide during Sintering in a Reducing Atmosphere. *J. Am. Ceram. Soc.* **2018**, *101* (11), 4956–4967. https://doi.org/10.1111/jace.15741.

(13) Walter, O.; Popa, K.; Blanco, O. D. Hydrothermal Decomposition of Actinide(IV) Oxalates: A New Aqueous Route towards Reactive Actinide Oxide Nanocrystals. *Open Chem.* **2016**, *14* (1), 170–174. https://doi.org/10.1515/chem-2016-0018.

(14) Popa, K.; Walter, O.; Dieste Blanco, O.; Guiot, A.; Bouëxière, D.; Colle, J.-Y.; Martel, L.; Naji, M.; Manara, D. A Low-Temperature Synthesis Method for AnO_2 Nanocrystals (An = Th, U, Np, and Pu) and Associate Solid Solutions. *CrystEngComm* **2018**, *20* (32), 4614–4622. https://doi.org/10.1039/C8CE00446C.

(15) Balice, L.; Bouëxière, D.; Cologna, M.; Cambriani, A.; Vigier, J.-F.; De Bona, E.; Sorarù, G. D.; Kübel, C.; Walter, O.; Popa, K. Nano and Micro $U_{1-x}Th_xO_2$ Solid Solutions: From Powders to Pellets. *J. Nucl. Mater.* **2018**, *498*, 307–313. https://doi.org/10.1016/j.jnucmat.2017.10.042.
(16) Manaud, J.; Maynadié, J.; Mesbah, A.; Hunault, M. O. J. Y.; Martin, P. M.; Zunino, M.; Meyer, D.; Dacheux, N.; Clavier, N. Hydrothermal Conversion of Uranium(IV) Oxalate into Oxides: A Comprehensive Study. *Inorg. Chem.* **2020**, *59* (5), 3260–3273. https://doi.org/10.1021/acs.inorgchem.9b03672.
(17) Serp, J.; Allibert, M.; Beneš, O.; Delpech, S.; Feynberg, O.; Ghetta, V.; Heuer, D.; Holcomb, D.; Ignatiev, V.; Kloosterman, J. L.; Luzzi, L.; Merle-Lucotte, E.; Uhlíř, J.; Yoshioka, R.; Zhimin, D. The Molten Salt Reactor (MSR) in Generation IV: Overview and Perspectives. *Prog. Nucl. Energy* **2014**, *77*, 308–319. https://doi.org/10.1016/j.pnucene.2014.02.014.
(18) Sinha, R. K.; Kakodkar, A. Design and Development of the AHWR—the Indian Thorium Fuelled Innovative Nuclear Reactor. *Nucl. Eng. Des.* **2006**, *236* (7), 683–700. https://doi.org/10.1016/j.nucengdes.2005.09.026.
(19) Zhang, D.; Liu, L.; Liu, M.; Xu, R.; Gong, C.; Zhang, J.; Wang, C.; Qiu, S.; Su, G. Review of Conceptual Design and Fundamental Research of Molten Salt Reactors in China. *Int. J. Energy Res.* **2018**, *42* (5), 1834–1848. https://doi.org/10.1002/er.3979.
(20) Rabenau, A. The Role of Hydrothermal Synthesis in Preparative Chemistry. *Angew. Chem. Int. Ed.* **1985**, *24* (12), 1026–1040. https://doi.org/10.1002/anie.198510261.
(21) Dzimitrowicz, D. J.; Wiseman, P. J.; Cherns, D. An Electron Microscope Study of Hydrous Thorium Dioxide ThO2 · NH2O. *J. Colloid Interface Sci.* **1985**, *103* (1), 170–177. https://doi.org/10.1016/0021-9797(85)90089-X.
(22) Thompson, P.; Cox, D. E.; Hastings, J. B. Rietveld Refinement of Debye–Scherrer Synchrotron X-Ray Data from Al_2O_3. *J. Appl. Crystallogr.* **1987**, *20* (2), 79–83. https://doi.org/10.1107/S0021889887087090.
(23) Frontera, C.; Rodríguez-Carvajal, J. FullProf as a New Tool for Flipping Ratio Analysis. *Phys. B Condens. Matter* **2003**, *335* (1), 219–222. https://doi.org/10.1016/S0921-4526(03)00241-2.
(24) Sitaud, B.; Solari, P. L.; Schlutig, S.; Llorens, I.; Hermange, H. Characterization of Radioactive Materials Using the MARS Beamline at the Synchrotron SOLEIL. *J. Nucl. Mater.* **2012**, *425* (1), 238–243. https://doi.org/10.1016/j.jnucmat.2011.08.017.
(25) LLorens, I.; Solari, P. L.; Sitaud, B.; Bes, R.; Cammelli, S.; Hermange, H.; Othmane, G.; Safi, S.; Moisy, P.; Wahu, S.; Bresson, C.; Schlegel, M. L.; Menut, D.; Bechade, J.-L.; Martin, P.; Hazemann, J.-L.; Proux, O.; Den Auwer, C. X-Ray Absorption Spectroscopy Investigations on Radioactive Matter Using MARS Beamline at SOLEIL Synchrotron. *Radiochim. Acta* **2014**, *102* (11), 957–972. https://doi.org/10.1515/ract-2013-2241.
(26) Ravel, B.; Newville, M. ATHENA, ARTEMIS, HEPHAESTUS: Data Analysis for X-Ray Absorption Spectroscopy Using IFEFFIT. *J. Synchrotron Radiat.* **2005**, *12* (4), 537–541. https://doi.org/10.1107/S0909049505012719.
(27) Hennig, C. Evidence for Double-Electron Excitations in the L_3-Edge x-Ray Absorption Spectra of Actinides. *Phys. Rev. B* **2007**, *75* (3), 035120. https://doi.org/10.1103/PhysRevB.75.035120.
(28) Clavier, N.; Hingant, N.; Rivenet, M.; Obbade, S.; Dacheux, N.; Barré, N.; Abraham, F. X-Ray Diffraction and μ-Raman Investigation of the Monoclinic-Orthorhombic Phase Transition in $Th_{1-x}U_x(C_2O_4)_2{\cdot}2H_2O$ Solid Solutions. *Inorg. Chem.* **2010**, *49* (4), 1921–1931. https://doi.org/10.1021/ic902343r.

(29) Dash, S.; Krishnan, R.; Kamruddin, M.; Tyagi, A. K.; Raj, B. Temperature Programmed Decomposition of Thorium Oxalate Hexahydrate. *J. Nucl. Mater.* **2001**, *295* (2), 281–289. https://doi.org/10.1016/S0022-3115(01)00481-0.
(30) Wendlandt, W. W.; George, T. D.; Horton, G. R. The Thermal Decomposition of Thorium(IV), Uranium(IV), and the Rare-Earth Metal(III) Oxalate Hydrates. Differential Thermal Analysis and Weight-Loss Studies. *J. Inorg. Nucl. Chem.* **1961**, *17* (3), 273–280. https://doi.org/10.1016/0022-1902(61)80151-6.
(31) Crossey, L. J. Thermal Degradation of Aqueous Oxalate Species. *Geochim. Cosmochim. Acta* **1991**, *55* (6), 1515–1527. https://doi.org/10.1016/0016-7037(91)90124-N.
(32) Rand, M. H.; Fuger, J.; Neck, V.; Grenthe, I.; Rai, D. *Chemical Thermodynamics of Thorium*, OECD NEA.; Chemical Thermodynamics; 2008; Vol. 11. https://doi.org/10.1787/9789264056688-en.
(33) Guillaumont, R.; Fanghänel, T.; Fuger, J.; Grenthe, I.; Neck, V.; Palmer, D. A.; Rand, M. H. *Update on the Chemical Thermodynamics of Uranium, Neptunium, Plutonium, Americium and Technetium*, OECD NEA.; Chemical Thermodynamics; 2003; Vol. 5.
(34) Bentouhami, E.; Bouet, G. M.; Meullemeestre, J.; Vierling, F.; Khan, M. A. Physicochemical Study of the Hydrolysis of Rare-Earth Elements (III) and Thorium (IV). *Comptes Rendus Chim.* **2004**, *7* (5), 537–545. https://doi.org/10.1016/j.crci.2004.01.008.
(35) Idiri, M.; Le Bihan, T.; Heathman, S.; Rebizant, J. Behavior of Actinide Dioxides under Pressure: UO_2 and ThO_2. *Phys. Rev. B* **2004**, *70* (1), 014113. https://doi.org/10.1103/PhysRevB.70.014113.
(36) Hubert, S.; Purans, J.; Heisbourg, G.; Moisy, P.; Dacheux, N. Local Structure of Actinide Dioxide Solid Solutions $Th_{1-x}U_xO_2$ and $Th_{1-x}Pu_xO_2$. *Inorg. Chem.* **2006**, *45* (10), 3887–3894. https://doi.org/10.1021/ic050888y.
(37) Morss, L. R.; Edelstein, N. M.; Fuger, J. *The Chemistry of the Actinide and Transactinide Elements (3rd Ed., Volumes 1-5)*; Springer Science & Business Media, 2007.
(38) Clavier, N.; Maynadié, J.; Mesbah, A.; Hidalgo, J.; Lauwerier, R.; Nkou Bouala, G. I.; Parrès-Maynadié, S.; Meyer, D.; Dacheux, N.; Podor, R. Thorium Aspartate Tetrahydrate Precursor to ThO_2: Comparison of Hydrothermal and Thermal Conversions. *J. Nucl. Mater.* **2017**, *487*, 331–342. https://doi.org/10.1016/j.jnucmat.2017.02.035.
(39) Plakhova, T. V.; Romanchuk, A. Yu.; Likhosherstova, D. V.; Baranchikov, A. E.; Dorovatovskii, P. V.; Svetogorov, R. D.; Shatalova, T. B.; Egorova, T. B.; Trigub, A. L.; Kvashnina, K. O.; Ivanov, V. K.; Kalmykov, S. N. Size Effects in Nanocrystalline Thoria. *J. Phys. Chem. C* **2019**, *123* (37), 23167–23176. https://doi.org/10.1021/acs.jpcc.9b04379.
(40) Bonato, L.; Virot, M.; Dumas, T.; Mesbah, A.; Dalodière, E.; Blanco, O. D.; Wiss, T.; Goff, X. L.; Odorico, M.; Prieur, D.; Rossberg, A.; Venault, L.; Dacheux, N.; Moisy, P.; I. Nikitenko, S. Probing the Local Structure of Nanoscale Actinide Oxides: A Comparison between PuO_2 and ThO_2 Nanoparticles Rules out PuO_{2+x} Hypothesis. *Nanoscale Adv.* **2020**, *2* (1), 214–224. https://doi.org/10.1039/C9NA00662A.
(41) Belle, J.; Berman, R. M. *Thorium Dioxide: Properties and Nuclear Applications*; DOE/NE--0060; 1984.
(42) Balakrishna, P.; Varma, B. P.; Krishnan, T. S.; Mohan, T. R. R.; Ramakrishnan, P. Thorium Oxide: Calcination, Compaction and Sintering. *J. Nucl. Mater.* **1988**, *160* (1), 88–94. https://doi.org/10.1016/0022-3115(88)90012-8.

(43) Dash, S.; Singh, A.; Ajikumar, P. K.; Subramanian, H.; Rajalakshmi, M.; Tyagi, A. K.; Arora, A. K.; Narasimhan, S. V.; Raj, B. Synthesis and Characterization of Nanocrystalline Thoria Obtained from Thermally Decomposed Thorium Carbonate. *J. Nucl. Mater.* **2002**, *303* (2), 156–168. https://doi.org/10.1016/S0022-3115(02)00816-4.
(44) Desfougeres, L.; Welcomme, É.; Ollivier, M.; Martin, P. M.; Hennuyer, J.; Hunault, M. O. J. Y.; Podor, R.; Clavier, N.; Favergeon, L. Oxidation as an Early Stage in the Multistep Thermal Decomposition of Uranium(IV) Oxalate into U3O8. *Inorg. Chem.* **2020**, *59* (12), 8589–8602. https://doi.org/10.1021/acs.inorgchem.0c01047.
(45) White, G. D.; Bray, L. A.; Hart, P. E. Optimization of Thorium Oxalate Precipitation Conditions Relative to Derived Oxide Sinterability. *J. Nucl. Mater.* **1981**, *96* (3), 305–313. https://doi.org/10.1016/0022-3115(81)90574-2.
(46) Tyrpekl, V.; Vigier, J.-F.; Manara, D.; Wiss, T.; Dieste Blanco, O.; Somers, J. Low Temperature Decomposition of U(IV) and Th(IV) Oxalates to Nanograined Oxide Powders. *J. Nucl. Mater.* **2015**, *460*, 200–208. https://doi.org/10.1016/j.jnucmat.2015.02.027.
(47) Martinez, J.; Clavier, N.; Ducasse, T.; Mesbah, A.; Audubert, F.; Corso, B.; Vigier, N.; Dacheux, N. From Uranium(IV) Oxalate to Sintered UO_2: Consequences of the Powders' Thermal History on the Microstructure. *J. Eur. Ceram. Soc.* **2015**, *35* (16), 4535–4546. https://doi.org/10.1016/j.jeurceramsoc.2015.07.010.
(48) Orr, R. M.; Sims, H. E.; Taylor, R. J. A Review of Plutonium Oxalate Decomposition Reactions and Effects of Decomposition Temperature on the Surface Area of the Plutonium Dioxide Product. *J. Nucl. Mater.* **2015**, *465*, 756–773. https://doi.org/10.1016/j.jnucmat.2015.06.058.
(49) Tyrpekl, V.; Beliš, M.; Wangle, T.; Vleugels, J.; Verwerft, M. Alterations of Thorium Oxalate Morphology by Changing Elementary Precipitation Conditions. *J. Nucl. Mater.* **2017**, *493*, 255–263. https://doi.org/10.1016/j.jnucmat.2017.06.027.
(50) Trillaud, V.; Maynadié, J.; Manaud, J.; Hidalgo, J.; Meyer, D.; Podor, R.; Dacheux, N.; Clavier, N. Synthesis of Size-Controlled UO_2 Microspheres from the Hydrothermal Conversion of U(Iv) Aspartate. *CrystEngComm* **2018**, *20* (48), 7749–7760. https://doi.org/10.1039/C8CE01352G.
(51) Blanchard, F.; Rivenet, M.; Vigier, N.; Hablot, I.; Grandjean, S.; Abraham, F. Solid State Chemistry of Ten-Fold Coordinate Thorium(IV) Complexes with Oxalates in the Presence of Ammonium and Hydrazinium Ions. *Cryst. Growth Des.* **2018**, *18* (8), 4593–4601. https://doi.org/10.1021/acs.cgd.8b00565.
(52) Neck, V.; Kim, J. I. Solubility and Hydrolysis of Tetravalent Actinides. *Radiochim. Acta* **2001**, *89* (1), 1–16. https://doi.org/10.1524/ract.2001.89.1.001.
(53) Bertolo, L. A.; Shukla, M. M. A Calculation of Debye-Waller Factors for F.C.C. Metals. *Phys. Status Solidi B* **1976**, *77* (2), 433–439. https://doi.org/10.1002/pssb.2220770203.
(54) Pandya, T. C.; Vyas, P. R.; Pandya, C. V.; Gohil, V. B. On the Model Pseudopotential Approach to Calculate the Lattice Mechanical Properties of Thorium. *Czechoslov. J. Phys.* **2001**, *51* (1), 49–58. https://doi.org/10.1023/A:1026665823572.
(55) Shannon, R. D. Revised Effective Ionic Radii and Systematic Studies of Interatomic Distances in Halides and Chalcogenides. *Acta Crystallogr. Sect. A* **1976**, *32* (5), 751–767. https://doi.org/10.1107/S0567739476001551.

For Table of Contents only

Hydrothermal conversion of thorium oxalate into ThO_2 was explored. Treatments of more than 5 hours above 220°C are required to decompose oxalates, while pH > 1 must be considered to recover a precipitate. All the oxide samples presented residual carbon and water in the range of 0.2-0.3 wt.% and n ≈ 0.5, respectively. From PXRD and EXAFS, these impurities were trapped between elementary nanosized crystallites which could explain their tendency to self-assemble as spherical aggregates.